Paradoxical Roles of Peritumoral Hepatic Stellate Cells in Liver Tumorigenesis in Mice: Retarding Tumor Growth and Promoting Tumor Dissemination

Cheng Tian[1], Liyuan Li[1], Li Fan[1], Anthony Brown[1], Eric J. Norris[2], and Liqin Zhu[1]

[1]Department of Pharmaceutical Sciences, St. Jude Children's Research Hospital, Memphis, Tennessee, United States and [2]STEMCELL Technologies, Vancouver, BC, Canada

Keywords

Peritumoral microenvironment, hepatic spheroid cocultures; hepatocyte, non-parenchymal cell, hepatic stellate cells

Correspondence

Liqin Zhu, PhD, Department of Pharmaceutical Sciences, St. Jude Children's Research Hospital, 262 Danny Thomas Place, Memphis, Tennessee 38105-3678. E-mail: liqin.zhu@stjude.org; fax: (901) 595-8869; tel: (901) 595-5250.

Abbreviations

WLC	Whole liver cells
HC	Hepatocyte
NPC	Nonparenchymal cell
pTME	Peritumoral microenvironment
HSC	Hepatic stellate cell
pHSC	Peritumoral hepatic stellate cell
EC	Endothelial cell
KC	Kupffer cell
CC	Cholangiocyte
3D	Three-dimensional
CHC	Combined hepatocellular carcinoma and cholangiocarcinoma
Alb-cre; Rtd	Albumin-cre; Rosa-tdTomato
PPTR	Prom1^{CreERT2}; Pten$^{flx/flx}$; Tp53$^{flx/flx}$; Rosa-ZsGreen
IHC	Immunohistochemistry
ZsG	ZsGreen1
GFP	Green fluorescence protein
Rtd	Rosa-tdTomato
DTC	Disseminated tumor cell

Grant Support: This work was supported by American Cancer Society Research Scholar Grant RSG-18-026-01.

Disclosures: None declared.

Author Contributions: C.T. conducted most of the biological experiments. L.L., L.F., and A.B. conducted experiments. E.N. provided technical and intellectual support. L.Z. conceived and oversaw the research. All authors contributed to the writing of the manuscript.

Acknowledgements: We are grateful to the staff of the Animal Resource Center, Veterinary Pathology Core, and Cell and Tissue Imaging at St. Jude Children's Research Hospital for providing technical assistance.

Editing Assistance: Vani Shanker (PhD) at St. Jude Children's Research Hospital edited the manuscript for nonintellectual content.

ABSTRACT

Background and Rationale

Cancer is increasingly being viewed as an ecosystem in which tumor cells coevolve and cooperate with host cells. In liver cancer, extensive biological changes have been reported in parenchymal hepatocytes (HCs) and non-parenchymal cells (NPCs) in the peritumoral microenvironment (pTME). However, it remains controversial how individual pTME populations contribute to liver tumorigenesis. We aim to develop an efficient *in vitro* model system to dissect the intricate relationship between liver tumor and its surroundings.

Results

In this study, we established three-dimensional spheroid cocultures of primary mouse liver cells. We show that spheroids of HCs and NPCs can be readily generated in micropatterned multiwell plates. When cocultured with liver tumor spheroids, NPC spheroids, but not HC spheroids, exhibited a potent suppression activity on tumor cell growth. However, tumor cells (T) in NPC-T culture, while enduring growth suppression, showed a significant increase in dissemination compared to that in HC-T or T-alone culture. We then showed that hepatic stellate cells (HSCs) in NPCs are a key contributor to this NPC-mediated tumor growth suppression and dissemination augmentation. We validated our results in a highly metastatic orthotopic liver cancer allograft model. We showed that tumor development in this model induced widespread activation of HSCs in the pTME, and the accumulation of peritumoral HSCs at the tumor border is associated with retarded tumor growth and enhanced tumor dissemination.

Conclusion

This study reveals a paradoxical role of peritumoral HSCs in liver tumorigenesis beyond being simply pro- or anti-tumorigenic. Tumor development in mouse liver induces activation of peritumoral HSCs that effectively retard tumor growth but simultaneously promote tumor dissemination.

INTRODUCTION

It has been increasingly recognized that solid tumors are an ecosystem in which tumor cells cooperate with host cells in their peritumoral microenvironment (pTME). Studies have found widespread cellular and molecular changes in the pTME of many aggressive types of solid tumors (1-7). In liver cancer, the tumor-surrounding parenchyma is composed of hepatocytes (HCs) and nonparenchymal cells (NPCs) including endothelial cells (ECs), Kupffer cells (KCs), cholangiocytes (CCs), and hepatic stellate cells (HSCs). In the normal liver, HCs are responsible for most metabolic and hormonal processes and NPCs support the structure of the liver, transport molecules in and out, and communicate with the immune system (8). The tightly regulated teamwork from both compartments is known to be critical to normal liver development and function. However, their individual and coordinated responses to tumorigenesis are less explored. We reasoned that a comparative analysis of the interaction between liver tumor cells and HCs and NPCs in pTME is necessary for a comprehensive and accurate understanding of liver tumorigenesis.

Among different cancer models, *in vivo* animal models are indisputably the best at recapitulating systemic cancer development. However, *in vitro* cellular models are unique in their ability to rapidly assess the contribution of different cell populations to tumorigenesis. Recent developments in three-dimensional (3D) cellular models have greatly facilitated research efforts to model normal and malignant development *in vitro*, given their ability to closely mimic the 3D cellular organization of the actual tissue and retain relevant physiology (9). Organoid and spheroid models are the most commonly used 3D models among various 3D platforms developed over the years, likely because of their easy setup and high efficiency (10-14). For HCs, organoid models are not particularly robust probably due to the lack of a designated stem cell population supporting HC regeneration. On the other hand, HC spheroid models are easy to establish and a good platform to assess HC behaviors *in vitro* (15). Recent studies found that chemically defined serum-free medium similar to that used for organoid cultures can maintain the long-term phenotypical and biological stability of HC spheroids (16-18). For NPCs, they have been reported to increase the organization and drug resistance of HC spheroids (19, 20). Spheroids with only NPC lineages

have rarely been studied. Hence, there is a need to conduct more comparative studies on HC and NPC spheroids for their differential involvement in liver disease.

Current hepatic spheroid studies mostly use cells from humans and rats. Given the rich resource of genetically defined liver cancer mouse models, we reasoned that establishing mouse spheroid models from specific hepatic lineages would be beneficial to investigate the crosstalk between liver cancer and its pTME. Thus, in this study, we tested spheroid cultures of unfractionated whole liver cells (WLCs), HCs, and NPCs from *Albumin-cre; Rosa-tdTomato* (*Alb-cre; Rtd*) mice in a chemically defined serum-free medium, and then compared their interaction in a coculture with liver tumor spheroids derived from a *Prom1*^{CreERT2}*; Pten*$^{flx/flx}$*; Tp53*$^{flx/flx}$*; Rosa-ZsGreen* (PPTR) mouse model we previously reported (21). We have shown that primary liver tumor cells from this model generated highly metastatic orthotopic tumors recapitulating combined hepatocellular carcinoma and cholangiocarcinoma (CHC) in patients (22). Then, we focused on the HSC lineage within the NPC population to demonstrate their impact on tumor cell behaviors. Finally, we validated our observations from spheroid cultures *in vivo* in a PPTR orthotopic transplantation model established in *Alb-cre; Rtd* mice.

EXPERIMENTAL PROCEDURES

Mice and PPTR orthotopic transplantation model

Alb-cre; Rtd mice were generated by breeding the *Albumin-cre* strain (JAX 003574) and the *Rosa26-tdTomato (Rtd)* reporter strain (JAX 007914) from The Jackson Laboratory (Bar Harbor, ME, USA). Two-month-old *Alb-cre; Rtd* male and female mice were used in this study and showed no differences in results. All mice were maintained in the Animal Resource Center at St. Jude Children's Research Hospital (St. Jude). Mice were housed in ventilated, temperature- and humidity-controlled cages under a12-hr light/12-hr dark cycle and given a standard diet and water *ad libitum*. Liver tumor cells from the PPTR mouse model were cultured as previously described (22) and transplanted into the liver of *Alb-cre; Rtd* mice via surgical intrahepatic injection. Briefly, a midline longitudinal abdominal incision was made to expose the left lobe of the liver. Then, 1×10^5 PPTR tumor cells in 4 µl of 100% matrigel (Corning Inc, Corning, NY, USA) were injected in the liver parenchyma using a Hamilton syringe and needle (27 gauge/0.5 inch/12 degree bevel angle). Absorbable sutures were used to close the muscle wall, and tissue glue and wound clips were used to close the skin. Analgesic drugs were administrated during the surgery and the first week post the surgery. Animal protocols were approved by the St. Jude Animal Care and Use Committee.

Primary mouse liver cell isolation and culture

Liver cells were isolated from 2-month-old *Alb-cre; Rtd* mouse liver using the standard two-step collagenase perfusion method (23, 24). Briefly, mice were anesthetized with isoflurane, the liver was perfused with 30 ml of prewarmed EGTA solution (0.5 mM) through the inferior vena cava for 10 min, and then perfused with 30 ml of prewarmed pronase solution (14 mg/mouse; Sigma, St. Louis, MO, USA) followed by 30 ml of collagenase solution (3.7 U/mouse; Roche, Basel, Switzerland) for 10 min each. The liver was then removed and transferred to a sterile Petri dish and gently minced with forceps. The liver was further digested with the pronase/collagenase solution with 1% DNase I (Sigma-Aldrich) for 25 min at 40 °C. Cells were filtered by a 70-µm filter and used directly as unfractionated WLCs, or centrifugated

at 50 ×*g* for 3 min to pellet HCs. The supernatant was then centrifuged at 580 ×*g* for 5 min to pellet NPCs. WLCs, HCs, and NPCs were washed twice in cold Advanced DMEM/F12 (Thermo Fisher Scientific, Waltham, MA, USA) and subjected to spheroid culture.

Generation of mouse liver spheroid

WLCs, HCs, and NPCs were seeded in 24-well AggreWell 400 (AW400) culture plates (STEMCELL Technologies, Vancouver, Canada) at 125, 250, 500, and 1000 cells/microwell, and 24-well AggreWell 800 plates at 500, 1000, and 2000 cells/microwell for 7 days according to the manufacturer's instructions. PPTR tumor cells were seeded at 125 cells/microwell in AW400 plates and cultured for 2 days. The same culture medium was used for all spheroid cultures: 50% mouse HepatiCult™ Organoid Growth Medium (STEMCELL), 50% CC organoid culture medium reported previously, and 1% matrigel (25). The CC organoid culture medium was prepared by supplementing advanced DMEM/F12 (Thermo Fisher) with 50% conditioned medium from L-WRN cells (ATCC CRL-3276™, Manassas, VA, US), 10 mM HEPES, 1% GlutaMax, 1% Penicillin-Streptomycin, 2% B27 (Thermo Fisher), 1% N2 (Thermo Fisher), 3 μm CHIR99021 (Sigma-Aldrich), 1.25 mM N-acetylcysteine (Sigma-Aldrich), 10 mM Nicotinamide (Sigma-Aldrich), 10 nM recombinant gastrin (Sigma-Aldrich), 50 ng/ml EGF (Peprotech), 50 ng/ml FGF7 (Peprotech), 50 ng/ml FGF10 (Peprotech), 25 ng/ml HGF (Peprotech), 1 μM A83-01 (Tocris, Bristol, UK), 10 μM Rho Inhibitor γ-27632 (STEMCELL), and 1% growth factor-reduced matrigel.

Mouse spheroid cocultures

WLC, HC, and NPC spheroids were collected by low-speed centrifugation, mixed with tumor spheroids at a ratio of 15:1, 5:1, or 2:1 in 96-well U-bottom plates, and cultured for an additional 7 days with the same culture medium. All cultures were kept under continuous shaking at 80 rpm on a CO_2-resistant Orbital shaker (Thermo Fisher). To assess the impact of HSCs on tumor cell growth and dissemination, freshly isolated HCs from *Alb-cre; Rtd* mice were mixed with primary mouse HSCs (ScienCell Research Laboratories, Carlsbad, CA, USA) at a ratio of HC-only, 8:2, 5:5, 2:8, and HSC-only

in 96-well flat-bottom microplates. The plates were precoated with 1% matrigel and 1×10^4 total cells were seeded in each well. The culture medium was a mixture of 80% mouse HepatiCult™ Organoid Growth Medium (STEMCELL) and 20% Stellate Cell Medium (ScienCell). After cells attached after 24 hr, 2–3 PPTR tumor spheroids/well were seeded on top and cultured for an additional 14 days with the same culture medium.

Microscopy and GFP quantification

Liver spheroid formation in AggreWell plates and their interaction in cocultures were monitored daily by using an ECLIPSE Ts2R fluorescence microscope (Nikon, Minato City, Tokyo, Japan). Images were captured by NIS-Elements (Nikon). The ZsG^+ tumor cell area in their cocultures was measured by ImageJ and plotted in GraphPad Prism 7.

Immunohistochemistry analysis

Liver spheroids and tissues were fixed in neutral buffered formalin for 1 day at room temperature and submitted to HistoWiz Inc. (Brooklyn, NY) for paraffin processing and sectioning. Paraffin sections (4 μm) were analyzed by direct fluorescence microscopy, H&E staining, and immunohistochemistry (IHC). IHC antibodies included anti-Ki67 (Abcam, Cambridge, MA, USA, ab16667, 1:200); anti-CK19 (Abcam, ab133496, 1:250); anti-Vimentin (Abcam, ab92547, 1:500); anti-HNF4a (R&D System, Minneapolis, MN, USA, PP-K9218-00, 1:125); anti-Cyp3A (Abcam, ab3572, 1:500); anti-aSMA (Abcam, ab124964, 1:1000); and anti-CD68 (Abcam, ab125212, 1:1000). Direct ZsG and Rtd fluorescence images were taken from each section prior to IHC.

Statistical analysis

A two-tailed student t test was performed in GraphPad to compare two independent pairs of groups. A one-way ANOVA was performed when two or more groups were compared. A $P \leq 0.05$ was considered statistically significant. Survival curves and median survival of the PPTR orthotopic allograft models were determined by the Kaplan–Meier method in GraphPad.

RESULTS

Generation and characterization of mouse primary WLC, HC, and NPC spheroids

Single-cell suspension of whole liver cells was obtained from *Alb-Cre; Rtd* mice by standard two-step *in vivo* digestion (23). HCs and NPCs were then segregated from WLCs by low-speed centrifugation (**Suppl Fig. 1**). Generation of WLCs, HCs, and NPCs spheroids was optimized by seeding in AggreWell 400 (AW400) plates at 125, 250, 500, 1000 cells/microwell and AggreWell 800 (AW800) plates at 500, 1000, and 2000 cells/microwell. A 1:1 mixture of HepatiCult organoid culture medium (STEMCELL) and a reported CC organoid culture medium was used in all cultures to maintain an inclusive and consistent spheroid culture condition for various hepatic lineages. We found that WLCs and HCs behaved similarly and formed spheroids consistently at 125 cells/microwell in AW400 plates. WLCs and HCs behaved similarly at this seeding density, aggregating and forming solid Rtd^+ spheroids after 24–48 hr of incubation (**Fig. 1A, B**). WLC spheroid were slightly more heterogeneous, likely due to their more complex cellular composition. Seeding densities higher than 250 cells/microwell prevented HC and WLC aggregation (**Fig. 1A, B**). NPCs aggregated poorly at low densities, likely due to their much smaller sizes than HCs. NPCs at 2000 cells/microwell in AW800 plates showed the most consistent spheroid formation and produced spheroids relatively homogenous in shape and size in 5–7 days (**Fig. 1C**). In contrast to solid HC and WLC spheroids, NPC spheroids were mostly hollow in structure. NPC spheroids, similar to WLC and HC spheroids, were strongly Rtd^+, as it has been reported that *Alb-Cre* expression turns on floxed reporter genes in both HC and CC lineages (26).

WLC, HC, and NPC spheroids were collected after 7 days in culture, paraffin processed, and underwent H&E and IHC characterization: Cyp3A for differentiated HCs, HNF4a for HCs and hepatic progenitors, αSMA for activated HSCs, CD68 for KCs, and CK19 for CCs and Ki67 for proliferating cells (**Fig. 2**). We observed that although similar in their cellular organization, WLC spheroids exhibited a better maintenance of HC characteristics than HC spheroids. Both Cyp3A and HNF4a showed more intense staining in WLC spheroids than HC spheroids. We also found that many HCs in HC spheroids expressed a low level of CK19 that did not occur in HCs in WLC spheroids, suggesting a low level of HC

dedifferentiation under this culture condition when NPCs are absent. There were also rare HC spheroids consisting of predominantly Ki67$^+$/CK19$^+$ cells that acquired an entirely CC-like ductal structure, which were likely derived from rare stem-like HCs that possess a high regenerative capacity (**Suppl Fig. 2**) (27-29). CD68$^+$ KCs, aSMA$^+$ HSCs, and CK19$^+$ CCs were found in WLC spheroids but not in HC spheroids, and all showed a higher content in NPC spheroids as expected. Interestingly, the cellular organization of NPC spheroids is somewhat similar to that of liver sinusoids, with CD68$^+$ KCs located in the outermost layer, αSMA$^+$ HSCs in the middle layer, and CK19$^+$ CCs in the inner layer. A small number of HNF4a$^+$ cells were also found in NPC spheroids. These cells did not express any other markers, and therefore were potentially dedifferentiated hepatic progenitors. Cells in WLC and HC spheroids were rarely proliferating compared to approximately 10–20% Ki67$^+$ cells in NPC spheroids (**Fig. 2**). We also performed CD31 IHC but did not detect CD31$^+$ ECs in any spheroids (data not shown).

NPCs, not HCs, suppress tumor cell proliferation but induce tumor cell dissemination in spheroid coculture

As we were successful in generating large numbers of WLC, HC, and NPC spheroids, we next tested their cocultures with mouse liver tumor spheroids to model tumor–pTME interaction *in vitro*. We have previously reported the establishment of multiple metastatic liver cancer organoid lines from a PPTR liver cancer mouse model (21, 22). Their tumor cells express a strong ZsGreen (ZsG) green fluorescent protein (GFP) from a genetically introduced *Rosa-ZsG* reporter allele. Although organoid cultures of these tumor cells were efficient, their organoids were heterogeneous in size and shape (**Suppl Fig. 3**). To acquire homogenous 3D cellular structures of these tumor cells to reproducibly assess their interaction with normal liver spheroids, we tested the efficiency of tumor spheroid generation using the same culture conditions in AW400 plates. We found that homogenous PPTR spheroids could be readily generated within 48 hr in culture at 125 cells/microwell in AW400 plates (**Fig. 3A**).

Tumor cell spheroids were then collected after 48 hr and mixed with WLC, HC, or NPC spheroids in 96-well U-bottom microplates in suspension. The same medium was used for cocultures.

Spheroid density could be determined in suspension, but we found it technically difficult to dispense an exact number of spheroids due to the difficulty in maintaining a homogeneous spheroid suspension solution during transfer. We first mixed the tumor spheroids with WLC, HC, or NPC spheroids at a ratio of 1:15, or tumor spheroids alone, referred to as WLC-T, HC-T, NPC-T, and T-only culture, respectively (**Fig. 3B**). Cocultures were continuously monitored for 7 days. We found that in all four conditions, spheroids aggregated and fused into one large spheroid by 48 hr. Spheroid fusion occurred most rapidly in the HC-T culture and most slowly in the NPC-T culture (**Fig. 3B**). After spheroid fusion, we noticed a drastic difference in the tumor cell expansion rate in these cocultures. ZSG^+ areas occupied by tumor cells expanded rapidly in T-only and HC-T cultures at similar rates, more slowly in WLC-T culture, and interestingly, showed minimal increase in NPC-T cultures (**Fig. 3B, C,** and **Suppl Fig. 4**). To confirm this observation, we repeated the cocultures at an increased tumor:normal spheroid ratio of 1:5, mixing approximately 10 tumor spheroids with 50 HC or NPC spheroids per well in 96-well microplates. Again, we found a significantly faster expansion of the ZSG^+ tumor area in the HC-T culture compared to that in the NPC-T culture (**Fig. 3D**). To confirm that tumor cells proliferate more slowly when cocultured with NPCs than with HCs, paraffin sections from HC-T (5:1) and NPC-T (5:1) spheroids were prepared after 7 days of culture and stained for the cell proliferation marker Ki67. As expected, there was a significantly higher percentage of $Ki67^+$ tumor cells in HC-T spheroids than in NPC-T spheroids (35.4±3.1% vs. 10.0±2.5%, P=0.0004) (**Fig. 3E, F**)`.

Although tumor proliferation was suppressed in the NPC-T culture, we observed evident tumor cell dissemination in the NPC-T culture, especially when a high tumor:normal spheroid mixing ratio was used. At a ratio of 1:2, ZSG^+ disseminated tumor cells (DTCs) were evident at 48 hr in the NPC-T culture when tumor spheroids started to fuse with NPC spheroids. ZSG^+ DTCs continued to increase in the NPC-T culture with longer coculturing (**Fig. 4A**). Such dissemination was also observed in WLC-T culture, but at a lower extent. The HC-T culture showed very limited DTCs and the T-only culture never had tumor cells disseminated within the 7 days of coculturing (**Fig. 4B**).

HSCs are a major contributor to the NPC-mediated tumor growth suppression and tumor dissemination induction

To elucidate the interaction between different NPC lineages and tumor cells in spheroid cocultures, we first performed IHC characterization of αSMA$^+$ HSCs, CK19$^+$ CCs, and CD68$^+$ KCs in WLC-T and NPC-T spheroids. We found that, interestingly, there was an evident accumulation of αSMA$^+$ HSCs in the areas where there was the least tumor cell attachment and the fewest Ki67$^+$ proliferating tumor cells in WLC-T spheroids (**Fig. 5A**). We did not find such associations for CK19$^+$ CCs and CD68$^+$ KCs (**Suppl Fig. 5**). Accumulation of αSMA$^+$ HSCs was also consistently observed at the edge of NPC-T spheroids where there was no tumor cell attachment (**Fig. 5B**). However, compared to WLC-T spheroids, such accumulation was less evident in NPC-T spheroids despite NPC spheroids having higher HSC content than WLC spheroids prior to their coculturing with tumor spheroids (**Fig 2, and Suppl Fig. 6**). It is possible that the small size of NPC-T spheroids and low tumor cell content prevented us from fully visualizing the interaction between tumor and HSCs via paraffin section-based IHC.

Next, we sought to demonstrate whether the presence of peritumoral HSCs (pHSCs) contributed to the tumor growth suppression and tumor dissemination induction we observed in WLC-T and NPC-T cocultures. Since it was difficult to accurately assess live tumor cell behaviors in 3D suspension culture, we modified our coculture system by seeding a mixture of HC:HSC at different ratios, including HC-only, 8:2, 5:5, 2:8, and HSC-only in flat-bottom 96-well microplates. We let them attach for 24 hr and then seeded 2–3 tumor spheroids per well on the top. We observed that tumor spheroids started to flatten within a day after seeding and showed a rapid difference in their expansion rate under these conditions. Tumor spheroids expanded most rapidly on top of HC-only. Addition of HSCs in the bottom layer significantly slowed tumor cell expansion, with those seeded on top of HSC-only expanding at the slowest rate (**Fig. 5C, D**), consist with our findings from NPC-T spheroids. By day 4, tumor spheroids seeded on top of HC-only were approximately four times bigger than those on top of HSC-only. By day

14, tumor cells on HC-only had reached 80-90% confluency while that of the tumor cells on top of the HC-HSC mixtures and HSC-only was well below 50% (**Fig. 5C**). Although growing more slowly, tumor cells seeded on top of the HC-HSC mixtures exhibited invasive behaviors starting from day 4 (**Fig. 5C**). Fibroblast-like invading tumor cells emerged on the tumor spheroid surface, which slowly broke away from the tumor spheroid and became migrating DTCs with extending microvilli (**Fig. 5C**). Interestingly, such invasion-to-dissemination transition was more evident in tumor spheroids seeded on top of the HC-HSC mixtures than those on top of HSC-only (**Fig. 5E**). However, direct tumor cell dissemination was clearly most prominent in the HSC-only condition, suggesting that tumor cell dissemination may occur in a less invasion-dependent manner when there is strong suppression of tumor cell expansion from the surrounding pTME (**Fig. 5E**).

Tumor dissemination in PPTR orthotopic allograft model is associated with the accumulation of activated pHSCs

To validate whether our observations from the *in vitro* spheroid cocultures recapitulate *in vivo* liver tumorigenesis, we orthotopically transplanted PPTR tumor cells into the liver of *Alb-Cre; Rtd* mice to visualize tumor proliferation, invasion, and dissemination in the *in vivo* pTME. Both PPTR lines transplanted generated similar metastatic CHC, with a median survival of 90 and 122 days (**Fig. 6A, B**). Because of the strong ZsG fluorescence of PPTR tumor cells, we were able to directly visualize tumor cells in this allograft model. In PPTR allograft mice that developed metastasis, we found extensive tumor cell dissemination and, surprisingly, pHSC activation in the liver near and far from the tumor, indicating a widespread pTME response to tumorigenesis in this model (**Fig. 6C** and **Suppl Fig. 7**). At the invasive front, there were a large number of ZsG^+ DTCs accompanied by significant disruption of the Rtd^+ liver parenchyma (**Fig. 6D**). Consistent with our *in vitro* observation, there was significantly higher accumulation of αSMA^+ pHSCs at the invasive front compared to the noninvasive tumor front. Tumor cells at the invasive front also showed a significantly lower proliferation rate compared to those that were not invading (**Fig. 6E**). Therefore, consistent with our *in vitro* observations, these was a same correlation

between the accumulation of pHSCs and suppressed tumor proliferation and augmented tumor dissemination in the PPTR orthotopic allograft model. This proves that the *in vitro* coculture platform we established is able to correctly model tumor-pHSC interaction to certain extent.

DISCUSSION

Past studies have identified cellular and molecular changes in liver cancer pTME associated with patient prognosis (3, 5, 6). However, research efforts on understanding the impact of individual pTME elements to liver tumorigenesis are limited. While *in vivo* liver cancer models are the most faithful research tool recapitulating liver tumorigenesis, it remains difficult to utilize these models to unravel the roles of pTME players due to their constant and complex crosstalk and coordination. The liver spheroid coculture platform we present here provides a much needed research tool for detailed dissection of the interaction between tumor cells and individual pTME elements.

In this study, we report using AggreWell microplates to generate homogeneous hepatic spheroids from mouse primary WLCs, HCs, and NPCs at high efficiencies. Such approaches have been previously used to establish spheroids from rat HCs but not yet tested in the mouse system (30, 31). Our study showed that the size of the microwell and seeding density are two key determinants of the efficiency in generating liver spheroids. For HCs and WLC, 125–200 cells/microwell in AW400 plates is optimal to generate spheroids within 2 days. Compared to conventional 96-well microplate–based liver spheroid culture that require 1000–1500 HCs per well (16, 32, 33), this method requires fewer HCs to generate a large number of homogeneous spheroids for downstream applications. Although WLCs and HCs aggregate similarly, we found that WLC spheroids maintained HC differentiation better than did HC spheroids. We detected widespread but weak expression of CK19 in HC spheroids, but not in WLC spheroids, after 7 days of culture (**Fig. 2**). HC-to-CC trans-differentiation or HC-to-hepatic progenitor dedifferentiation has been reported both *in vitro* and *in vivo* (27-29). Our results suggest that the presence of NPCs can help stabilize HCs *in vitro*. Spheroids consisting entirely of NPCs have not yet been reported. We found 2000 cells/microwell in AW800 plates as the optimal condition for NPCs to form

spheroids. CCs, HSCs, and KCs were preserved in our NPC spheroids and showed an organization somewhat similar to that for *in vivo* liver sinusoids. We did not detect ECs in NPC spheroids, suggesting that either we did not efficiently isolate ECs or our culture condition is not ideal for maintaining this critical NPC lineage. Hepatic ECs are known to be challenging to isolate and culture (34). Further optimization is required to allow the integration of ECs into NPC spheroids. Although generating hepatic spheroids is efficient by this approach, we found that a major technical challenge for their downstream applications is the transfer and reseeding of these spheroids. The difficulty in maintaining a homogeneous spheroid suspension during transfer can cause uneven seeding of spheroids for subsequent coculturing. Therefore, developing a robotic system for precise picking and seeding of spheroids into microplates will be beneficial to any high-throughput applications in the future.

Our cocultures of normal liver spheroids and PPTR liver tumor spheroids, to our knowledge, are one of first attempts to model the interaction between liver tumor and its pTME *in vitro*. We found that HC spheroids fused rapidly with tumor spheroids but had little effect on tumor cell growth. HCs were largely eliminated by the end of 7 days in coculture with tumor spheroids. In contrast, NPC spheroids showed not only a much slower fusion with tumor spheroids but also a very effective suppression on tumor cell proliferation. There was very limited growth for tumor spheroids cocultured with NPC spheroids within 7 days. However, interestingly, tumor cells showed marked dissemination in NPC-T cultures once the spheroids fused. DTCs were also present in the WLC-T culture but in lower numbers, were further reduced in HC-T cultures, and were completely absent in T-only cultures. We then showed that HSCs in the NPC population were a prime mediator of this dual function of NPCs on tumor cells: proliferation suppression and dissemination induction. In a modified coculturing system, when mixed HCs and HSCs were seeded as the bottom layer and tumor spheroids on the top, there was an evident increase in the suppression of tumor cell proliferation and promotion of tumor cell dissemination with increasing HSC content in the bottom layer. Lastly, we analyzed the PPTR orthotopic allograft model generated in *Alb-Cre; Rtd* mice to validate our *in vitro* observations. This allograft model is unique as it allows the direct visualization of tumor invasion and dissemination because of the strong Rtd expressed

by the liver parenchyma and ZsG from tumor cells. Similar to our spheroid cocultures, metastatic tumors generated in this model consistently showed the accumulation of activated pHSCs at the invasive front, accompanied by the slow tumor proliferation but extensive tumor dissemination comparing to the fast-growing but non-invading tumor cells at the non-invasive tumor border.

Changes in peritumoral NPC populations, including pHSC activation, have been reported in liver cancer patients, and studies have predominantly shown that these changes are protumorigenic and prometastatic (3, 35-39). However, based on our study, we propose that NPC-associated changes in the peritumoral liver are a defensive mechanism, at least at the early tumor development stage, to retard tumor development in order to preserve liver function. Therefore, it remains to be further evaluated whether or not targeting HSCs can be an effective therapeutic approach as previously proposed. Indeed, recent studies have started to argue that cirrhosis, a late-stage liver fibrosis condition that heavily involves HSC activation, may be a liver-protective response rather than a risk factor for live cancer (40). Studies in other solid tumors have also shown that deleting fibroblasts can accelerate tumor progression (41, 42). It has been widely recognized that NPCs respond rapidly to liver-damaging stimuli and induce liver repair via various mechanisms. Similar responses are likely elicited from pHSCs to tumor development to retard tumor growth and protect HC-dependent liver function because HCs, as our study showed, can be rapidly eliminated by tumor cells when they are in contact. However, an adverse consequence of such suppression is the promotion of aggressive cancer cell behaviors such as invasion and dissemination (43).

Overall, our study shows tumor-pHSC interaction is beyond simple pro- or anti-tumorigenic. There is tumor growth suppression at the early stage and tumor dissemination induction at the late stage mediated by tumor-pHSC interaction. Future studies are in line to identify specific mechanisms accounting for these behavioral changes. Optimizing this liver spheroid coculture platform is also necessary to include additional tumor and stromal lineages, such as ECs and immune cells, to understand their individual and joint contributions to liver tumorigenesis. Such a manipulatable 3D platform will provide the much-needed tool to dissect the complex and systemic changes in liver cancer pTME and facilitate a better understanding of clinical observations in liver cancer patients.

FIGURE LEGENDS

Figure 1. Generation of WLC, HC, and NPC spheroids in micropatterned AggreWell plates.

(A) Day 1 and Day 7 images of *Alb-Cre*; *Rtd* WLCs in AW400 plates seeded at the indicated density. BF: bright field; Rtd: tdTomato fluorescence. All images share the same 200 μm scale bar. ***(B)*** Day 1 and Day 7 images of *Alb-Cre*; *Rtd* HCs in AW400 plates seeded at the indicated density. All images share the same 200 μm scale bar. ***(C)*** Day 1 and Day 7 images of *Alb-Cre*; *Rtd* NPCs in AW400 and AW800 plates seeded at the indicated density. All images share the same 200 mm scale bar.

Figure 2. Immunohistochemical characterization of WLC, HC, and NPC spheroids using the indicated antibodies. All images share the same 100 μm scale bar.

Figure 3. NPC spheroids, not HC spheroids, suppress the growth of PPTR liver tumor spheroids in suspension cocultures.

(*A*) Formation of PPTR liver tumor spheroids in AW 400 plates. **(*B*)** Merged bright-field/ZsG/Rtd images of WLC-T, HC-T, and NPC-T spheroid cocultures at the indicated times after being transferred into 96-well plates. Rtd^+ normal spheroids and ZsG^+ tumor spheroids were mixed in a 15:1 ratio. **(*C*)** Percentage of ZsG^+ area occupied by tumor cells in each image from Day 0 to Day 7. ***(D)*** HC-T and NPC-T coculture with normal and tumor spheroids mixed at a 5:1 ratio. **(*E*)** ZsG/Rtd fluorescence microscopy and Ki67 IHC in HC-T and NPC-T spheroids collected 7 days after coculturing. ***(F)*** $Ki67^+$ cells in HC-T and NPC-T spheroids were quantified and compared by the t-test. $P < 0.001$.

Figure 4. NPCs induce tumor cell dissemination in spheroid suspension cocultures.

(*A*) Merged bright-field/ZsG images of WLC-T, HC-T, and NPC-T spheroid cocultures at the indicated times after being transferred into 96-well plates. Normal and tumor spheroids were mixed in a 2:1 ratio. All merged images share the same 200 μm scale bar. Images in the last column show the ZsG

fluorescence in the boxed area at 168 hr. Scale bars, 50 μm. ***(B)*** DTC quantification in indicated cocultures at 168 hr.

Figure 5. Peritumoral HSCs suppress tumor cell proliferation but promote tumor cell invasion and dissemination.

(*A*) ZsG/Rtd fluorescence microscopy and αSMA and Ki67 IHC on WLC-T spheroids collected 7 days after coculturing. Images on the same row share the same scale bar. **(*B*)** ZsG/Rtd fluorescence microscopy and αSMA IHC in NPC-T spheroids collected 7 days after coculturing. All images share the same scale bar. **(*C*)** Time-course ZsG fluorescence microscopy of tumor spheroids seeded on the top of HC:HSC mixed at the indicated ratio. Images on the same row share the same scale bar. **(*D*)** Tumor spheroid diameter from the indicated cocultures in (C) was measured from Day 0 to Day 4 and compared by two-way ANOVA in GraphPad. $P < 0.0001$. **(*E*)** Length of the tumor invading processes in indicated coculture conditions was measured and compared by two-way ANOVA in GraphPad. $P < 0.0001$.

Figure 6. Peritumoral HSCs are activated in the PPTR orthotopic allograft model and are associated with tumor cell growth suppression and dissemination promotion at the tumor invasive front.

(*A*) Survival curves of *Alb-Cre*; *Rtd* mice transplanted with two PPTR tumor cell lines. **(*B*)** The representative bright-field/ZsG images of the liver and lung harboring PPTR allograft tumors. **(*C*)** IHC of αSMA in the normal control liver vs. the liver harboring PPTR allograft tumors. Images on the same row share the same scale bar. **(*D*)** ZsG/Rtd fluorescence microscopy and αSMA and Ki67 IHC at the noninvasive and invasive border of PPTR allograft tumors. ***(E)*** $Ki67^+$ cells at the noninvasive and invasive tumor border were quantified and compared by the t-test. $P < 0.0001$.

REFERENCES

1. Xiong X, Kuang H, Ansari S, Liu T, Gong J, Wang S, Zhao XY, et al. Landscape of Intercellular Crosstalk in Healthy and NASH Liver Revealed by Single-Cell Secretome Gene Analysis. Mol Cell 2019;75:644-660 e645.
2. Madden E, AM G, SE L, A S. Tumour Cell Secretome in Chemoresistance and Tumour Recurrence. Trends in Cancer 2020.
3. Ji J, Eggert T, Budhu A, Forgues M, Takai A, Dang H, Ye Q, et al. Hepatic stellate cell and monocyte interaction contributes to poor prognosis in hepatocellular carcinoma. Hepatology 2015;62:481-495.
4. D'Alessio A, Proietti G, Sica G, Scicchitano BM. Pathological and Molecular Features of Glioblastoma and Its Peritumoral Tissue. Cancers (Basel) 2019;11.
5. Jiang J, Ye F, Yang X, Zong C, Gao L, Yang Y, Zhao Q, et al. Peri-tumor associated fibroblasts promote intrahepatic metastasis of hepatocellular carcinoma by recruiting cancer stem cells. Cancer Lett 2017;404:19-28.
6. Moya IM, Castaldo SA, Van den Mooter L, Soheily S, Sansores-Garcia L, Jacobs J, Mannaerts I, et al. Peritumoral activation of the Hippo pathway effectors YAP and TAZ suppresses liver cancer in mice. Science 2019;366:1029-1034.
7. Lee S, Zhou P, Gupta A, Shin S. Reactive Ductules Are Associated With Angiogenesis and Tumor Cell Proliferation in Pediatric Liver Cancer. Hepatol Commun 2018;2:1199-1212.
8. Malik R, Selden C, Hodgson H. The role of non-parenchymal cells in liver growth. Semin Cell Dev Biol 2002;13:425-431.
9. Tanner K, Gottesman MM. Beyond 3D culture models of cancer. Sci Transl Med 2015;7:283ps289.
10. Chatzinikolaidou M. Cell spheroids: the new frontiers in in vitro models for cancer drug validation. Drug Discov Today 2016;21:1553-1560.
11. Driehuis E, Kretzschmar K, Clevers H. Establishment of patient-derived cancer organoids for drug-screening applications. Nat Protoc 2020;15:3380-3409.
12. Sato T, Stange DE, Ferrante M, Vries RG, Van Es JH, Van den Brink S, Van Houdt WJ, et al. Long-term expansion of epithelial organoids from human colon, adenoma, adenocarcinoma, and Barrett's epithelium. Gastroenterology 2011;141:1762-1772.
13. Vlachogiannis G, Hedayat S, Vatsiou A, Jamin Y, Fernandez-Mateos J, Khan K, Lampis A, et al. Patient-derived organoids model treatment response of metastatic gastrointestinal cancers. Science 2018;359:920-926.
14. Tuveson D, Clevers H. Cancer modeling meets human organoid technology. Science 2019;364:952-955.
15. Mizoi K, Arakawa H, Yano K, Koyama S, Kojima H, Ogihara T. Utility of Three-Dimensional Cultures of Primary Human Hepatocytes (Spheroids) as Pharmacokinetic Models. Biomedicines 2020;8.
16. Bell CC, Hendriks DF, Moro SM, Ellis E, Walsh J, Renblom A, Fredriksson Puigvert L, et al. Characterization of primary human hepatocyte spheroids as a model system for drug-induced liver injury, liver function and disease. Sci Rep 2016;6:25187.
17. Vorrink SU, Zhou Y, Ingelman-Sundberg M, Lauschke VM. Prediction of Drug-Induced Hepatotoxicity Using Long-Term Stable Primary Hepatic 3D Spheroid Cultures in Chemically Defined Conditions. Toxicol Sci 2018;163:655-665.
18. Bao J, Fisher JE, Lillegard JB, Wang W, Amiot B, Yu Y, Dietz AB, et al. Serum-free medium and mesenchymal stromal cells enhance functionality and stabilize integrity of rat hepatocyte spheroids. Cell Transplant 2013;22:299-308.
19. Baze A, Parmentier C, Hendriks DFG, Hurrell T, Heyd B, Bachellier P, Schuster C, et al. Three-Dimensional Spheroid Primary Human Hepatocytes in Monoculture and Coculture with Nonparenchymal Cells. Tissue Eng Part C Methods 2018;24:534-545.

20. Bell CC, Chouhan B, Andersson LC, Andersson H, Dear JW, Williams DP, Soderberg M. Functionality of primary hepatic non-parenchymal cells in a 3D spheroid model and contribution to acetaminophen hepatotoxicity. Arch Toxicol 2020;94:1251-1263.
21. Zhu L, Finkelstein D, Gao C, Shi L, Wang Y, Lopez-Terrada D, Wang K, et al. Multi-organ Mapping of Cancer Risk. Cell 2016;166:1132-1146 e1137.
22. Li L, Qian M, Chen IH, Finkelstein D, Onar-Thomas A, Johnson M, Calabrese C, et al. Acquisition of Cholangiocarcinoma Traits during Advanced Hepatocellular Carcinoma Development in Mice. Am J Pathol 2018;188:656-671.
23. Berry MN, Friend DS. High-yield preparation of isolated rat liver parenchymal cells: a biochemical and fine structural study. J Cell Biol 1969;43:506-520.
24. Li WC, Ralphs KL, Tosh D. Isolation and culture of adult mouse hepatocytes. Methods Mol Biol 2010;633:185-196.
25. Hu H, Gehart H, Artegiani B, C LO-I, Dekkers F, Basak O, van Es J, et al. Long-Term Expansion of Functional Mouse and Human Hepatocytes as 3D Organoids. Cell 2018;175:1591-1606 e1519.
26. Malato Y, Naqvi S, Schurmann N, Ng R, Wang B, Zape J, Kay MA, et al. Fate tracing of mature hepatocytes in mouse liver homeostasis and regeneration. J Clin Invest 2011;121:4850-4860.
27. Guo R, Xu X, Lu Y, Xie X. Physiological oxygen tension reduces hepatocyte dedifferentiation in in vitro culture. Sci Rep 2017;7:5923.
28. Schaub JR, Huppert KA, Kurial SNT, Hsu BY, Cast AE, Donnelly B, Karns RA, et al. De novo formation of the biliary system by TGFbeta-mediated hepatocyte transdifferentiation. Nature 2018;557:247-251.
29. Michalopoulos GK, Bowen WC, Mule K, Lopez-Talavera JC, Mars W. Hepatocytes undergo phenotypic transformation to biliary epithelium in organoid cultures. Hepatology 2002;36:278-283.
30. Ijima H, Matsushita T, Nakazawa K, Fujii Y, Funatsu K. Hepatocyte Spheroids in Polyurethane Foams: Functional Analysis and Application for a Hybrid Artificial Liver. Tissue Engineering 2007;4:213–266.
31. Ha D, Thi PM, Chaudhary P, Jeong J. Efficient Formation of Three Dimensional Spheroids of Primary Hepatocytes Using Micropatterned Multi-Well Plates. Macromolecular Research 2019;27:938-943.
32. Nautiyal M, Qasem RJ, Fallon JK, Wolf KK, Liu J, Dixon D, Smith PC, et al. Characterization of primary mouse hepatocyte spheroids as a model system to support investigations of drug-induced liver injury. Toxicol In Vitro 2020;70:105010.
33. Kyffin JA, Sharma P, Leedale J, Colley HE, Murdoch C, Harding AL, Mistry P, et al. Characterisation of a functional rat hepatocyte spheroid model. Toxicol In Vitro 2019;55:160-172.
34. Poisson J, Lemoinne S, Boulanger C, Durand F, Moreau R, Valla D, Rautou PE. Liver sinusoidal endothelial cells: Physiology and role in liver diseases. J Hepatol 2017;66:212-227.
35. Budhu A, Forgues M, Ye QH, Jia HL, He P, Zanetti KA, Kammula US, et al. Prediction of venous metastases, recurrence, and prognosis in hepatocellular carcinoma based on a unique immune response signature of the liver microenvironment. Cancer Cell 2006;10:99-111.
36. Zhu XD, Zhang JB, Zhuang PY, Zhu HG, Zhang W, Xiong YQ, Wu WZ, et al. High expression of macrophage colony-stimulating factor in peritumoral liver tissue is associated with poor survival after curative resection of hepatocellular carcinoma. J Clin Oncol 2008;26:2707-2716.
37. Yang JD, Nakamura I, Roberts LR. The tumor microenvironment in hepatocellular carcinoma: current status and therapeutic targets. Semin Cancer Biol 2011;21:35-43.
38. Yin C, Evason KJ, Asahina K, Stainier DY. Hepatic stellate cells in liver development, regeneration, and cancer. J Clin Invest 2013;123:1902-1910.
39. Song Y, Kim SH, Kim KM, Choi EK, Kim J, Seo HR. Activated hepatic stellate cells play pivotal roles in hepatocellular carcinoma cell chemoresistance and migration in multicellular tumor spheroids. Sci Rep 2016;6:36750.

40. Garrido A, Djouder N. Cirrhosis: A Questioned Risk Factor for Hepatocellular Carcinoma. Trends Cancer 2021;7:29-36.
41. Rhim AD, Oberstein PE, Thomas DH, Mirek ET, Palermo CF, Sastra SA, Dekleva EN, et al. Stromal elements act to restrain, rather than support, pancreatic ductal adenocarcinoma. Cancer Cell 2014;25:735-747.
42. Ozdemir BC, Pentcheva-Hoang T, Carstens JL, Zheng X, Wu CC, Simpson TR, Laklai H, et al. Depletion of carcinoma-associated fibroblasts and fibrosis induces immunosuppression and accelerates pancreas cancer with reduced survival. Cancer Cell 2014;25:719-734.
43. Parker T, Madan E, Gupta K, Moreno E, Gogna R. Cell Competition Spurs Selection of Aggressive Cancer Cells. Trends Cancer 2020;6:732-736.

Figure 1

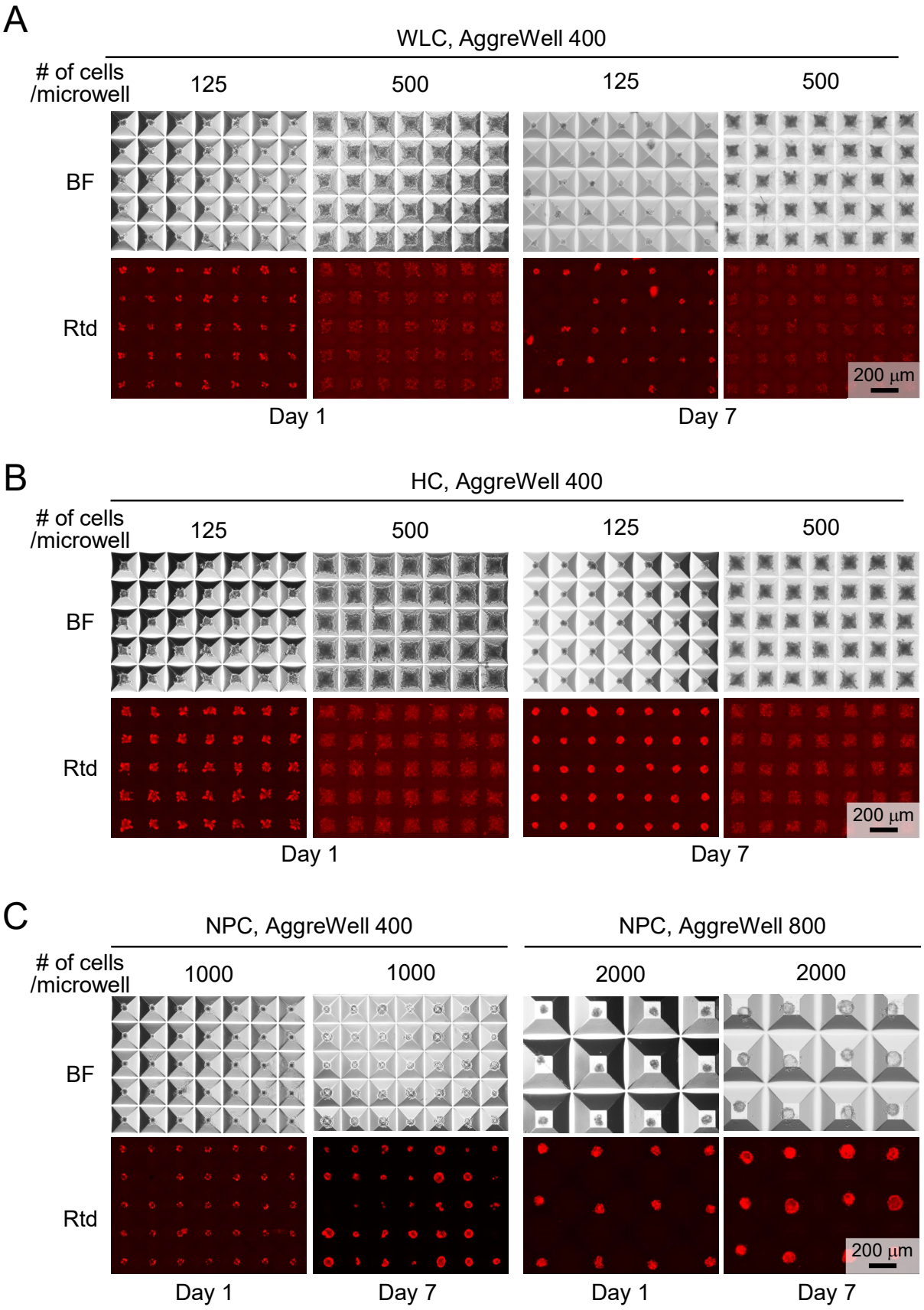
A
WLC, AggreWell 400
# of cells /microwell
125
500
125
500
BF
Rtd
200 µm
Day 1
Day 7
B
HC, AggreWell 400
# of cells /microwell
125
500
125
500
BF
Rtd
200 µm
Day 1
Day 7
C
NPC, AggreWell 400
NPC, AggreWell 800
# of cells /microwell
1000
1000
2000
2000
BF
Rtd
200 µm
Day 1
Day 7
Day 1
Day 7

Figure 2

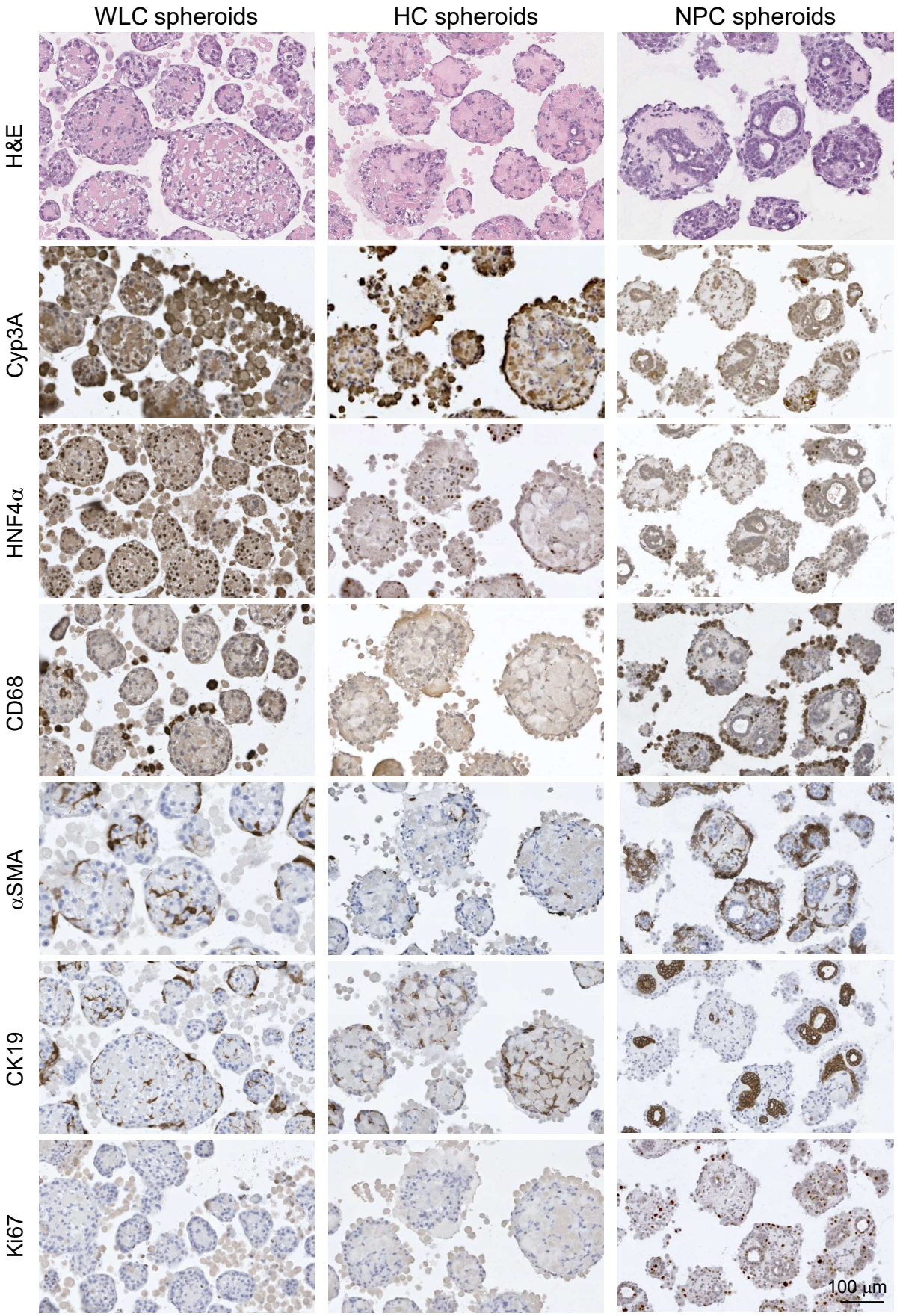
WLC spheroids
HC spheroids
NPC spheroids
H&E
Cyp3A
HNF4α
CD68
αSMA
CK19
Ki67
100 μm

Figure 3

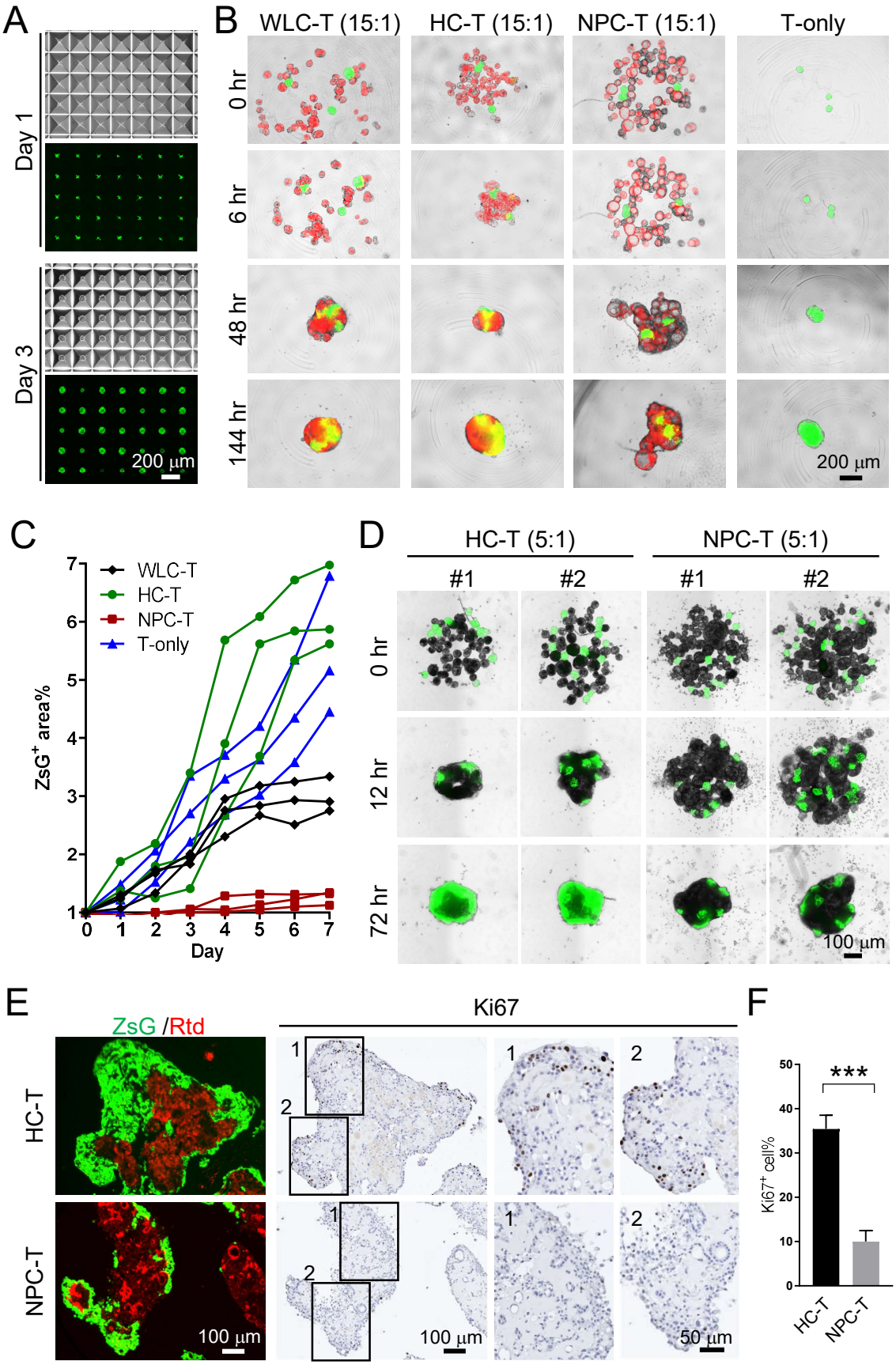
A
Day 1
Day 3
200 μm
B
WLC-T (15:1)
HC-T (15:1)
NPC-T (15:1)
T-only
0 hr
6 hr
48 hr
144 hr
200 μm
C
WLC-T
HC-T
NPC-T
T-only
ZsG+ area%
Day
D
HC-T (5:1)
NPC-T (5:1)
#1
#2
#1
#2
0 hr
12 hr
72 hr
100 μm
E
ZsG /Rtd
Ki67
HC-T
NPC-T
100 μm
100 μm
50 μm
F
***
Ki67+ cell%
HC-T
NPC-T

Figure 4

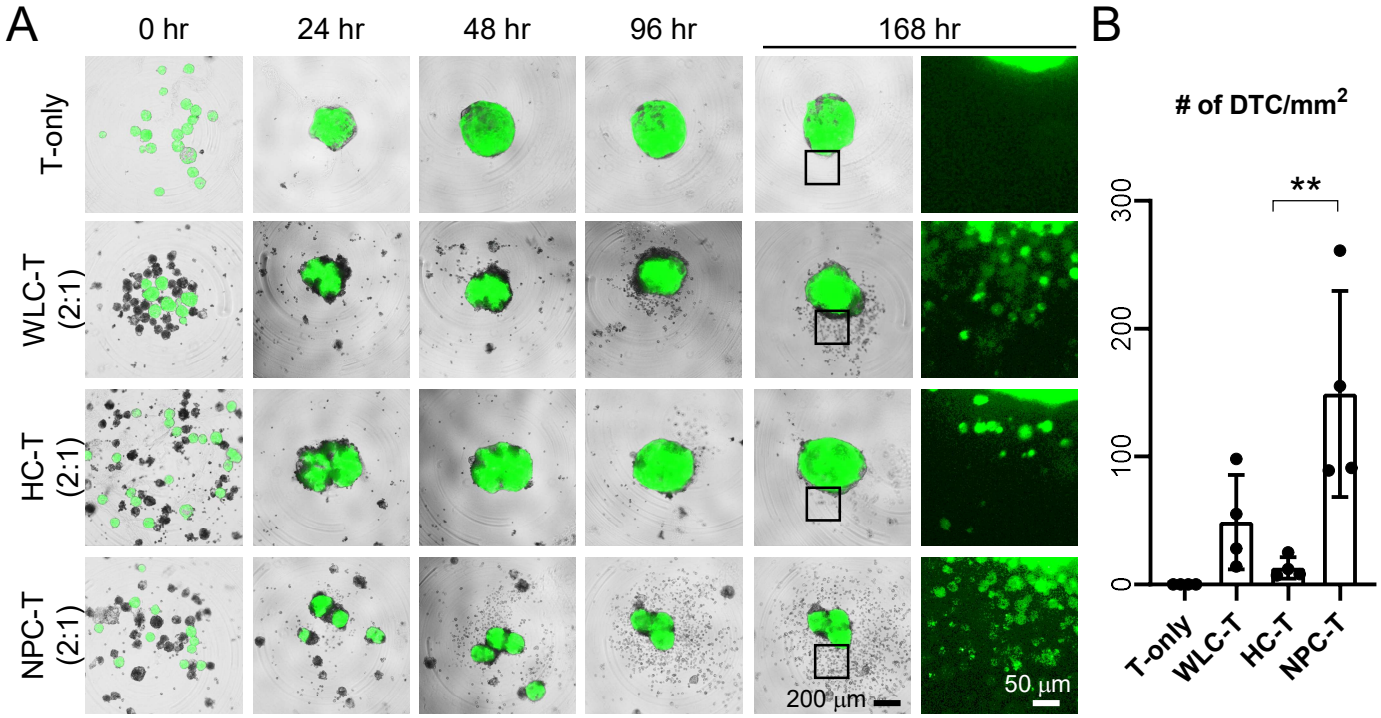
A
0 hr
24 hr
48 hr
96 hr
168 hr
T-only
WLC-T (2:1)
HC-T (2:1)
NPC-T (2:1)
200 µm
50 µm
B
# of DTC/mm2
**
300
200
100
0
T-only
WLC-T
HC-T
NPC-T

Figure 5

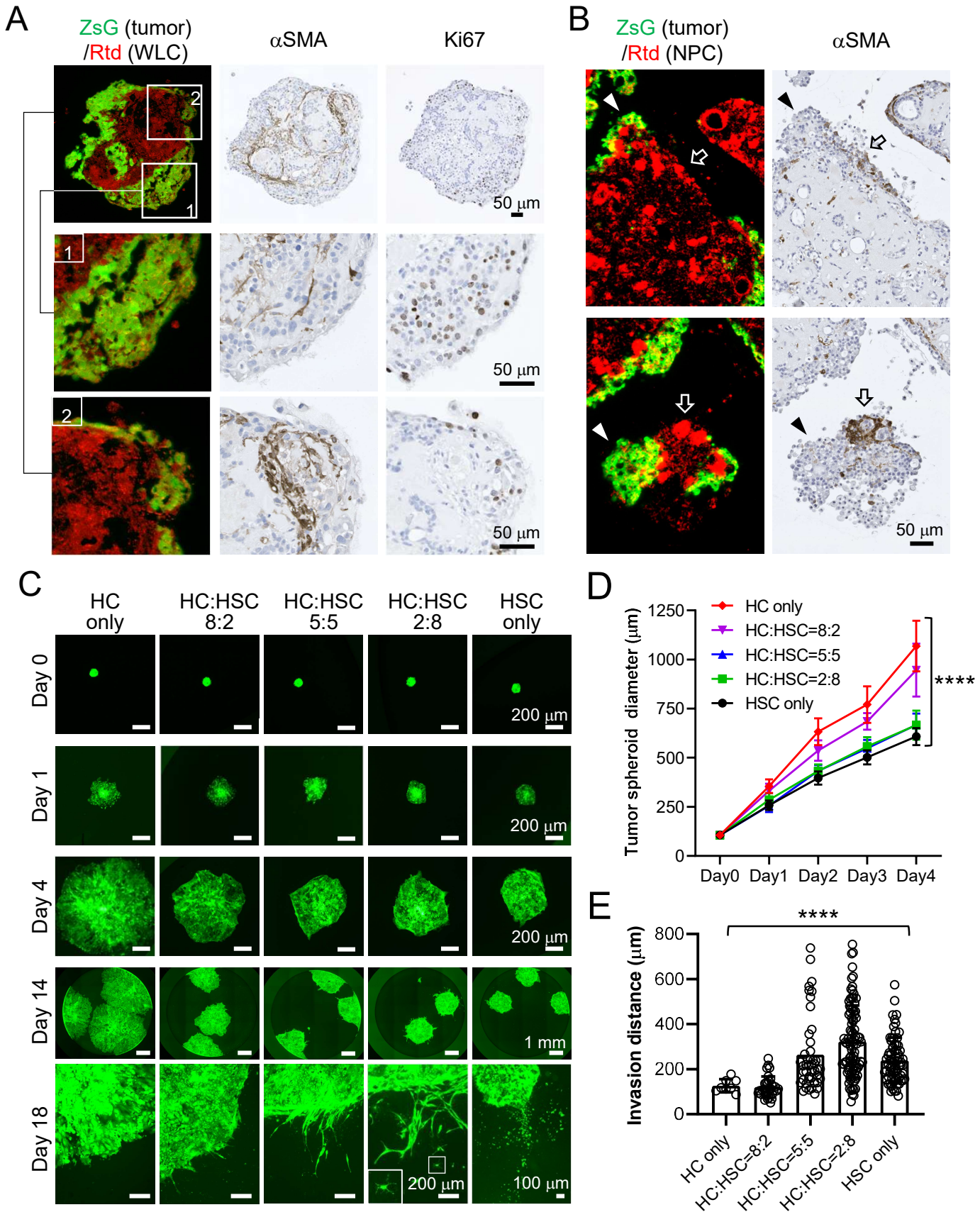
A
ZsG (tumor)
/Rtd (WLC)
αSMA
Ki67
2
1
1
2
50 μm
50 μm
50 μm
B
ZsG (tumor)
/Rtd (NPC)
αSMA
50 μm
C
HC only
HC:HSC 8:2
HC:HSC 5:5
HC:HSC 2:8
HSC only
Day 0
Day 1
Day 4
Day 14
Day 18
200 μm
200 μm
200 μm
1 mm
200 μm
100 μm
D
HC only
HC:HSC=8:2
HC:HSC=5:5
HC:HSC=2:8
HSC only
Tumor spheroid diameter (μm)
1250
1000
750
500
250
0
Day0
Day1
Day2
Day3
Day4
****
E
****
Invasion distance (μm)
800
600
400
200
0
HC only
HC:HSC=8:2
HC:HSC=5:5
HC:HSC=2:8
HSC only

Figure 6

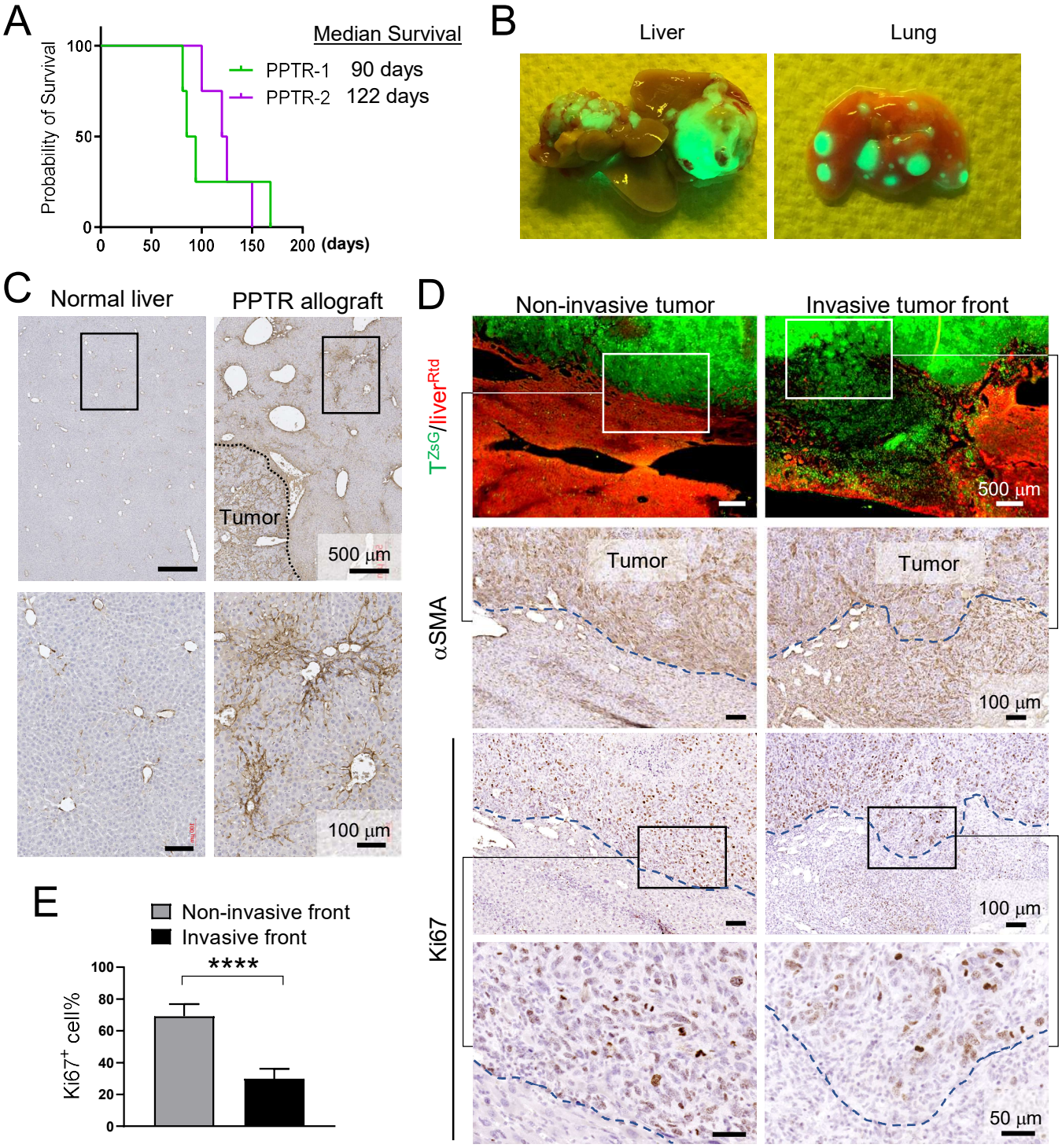
A
Median Survival
PPTR-1 90 days
PPTR-2 122 days
Probability of Survival
100
50
0
0
50
100
150
200 (days)
B
Liver
Lung
C
Normal liver
PPTR allograft
Tumor
500 µm
100 µm
D
Non-invasive tumor
Invasive tumor front
T^ZsG/liver^Rtd
500 µm
αSMA
Tumor
Tumor
100 µm
Ki67
100 µm
50 µm
E
Non-invasive front
Invasive front
****
Ki67+ cell%
100
80
60
40
20
0